

**W. J. Wang**

Department of Mechanical and  
Manufacturing Engineering  
De Montfort University,  
Leicester LE1 9BH, England

---

# Wavelet Transform in Vibration Analysis for Mechanical Fault Diagnosis

*The wavelet transform is introduced to indicate short-time fault effects in associated vibration signals. The time–frequency and time–scale representations are unified in a general form of a three-dimensional wavelet transform, from which two-dimensional transforms with different advantages are treated as special cases derived by fixing either the scale or frequency variable. The Gaussian enveloped oscillating wavelet is recommended to extract different sizes of features from the signal. It is shown that the time–frequency and time–scale distributions generated by the wavelet transform are effective in identifying mechanical faults. © 1996 John Wiley & Sons, Inc.*

---

## INTRODUCTION

In mechanical signal analysis, an ordinary power spectrum provides a description of the frequency distribution for the signal. Each frequency component is a collective contribution from all sections of the analysis duration; therefore it does not convey any information about when a frequency component appears or how it varies with time. Instead, decomposing a time signal into a time–frequency domain or time–scale domain gives information about the time development of frequency components. This property of time–frequency localization is particularly useful in representing short-duration signal components. Many mechanical faults, such as cracks, produce abnormal transients in the associated vibration signal due to shock or impact when the damaged surface of faulty mechanical elements is engaged. To provide this time information, the time–frequency synchronous representation (Classen and Mecklenbräuker, 1980) has been in-

roduced to the analysis of signals. Wang and McFadden (1993a,b) introduced the Gabor spectrogram for gear tooth damage detection and the method has been demonstrated as being very effective. All the features corresponding to a whole gear revolution can be represented by a single display on a time–frequency plane; gear faults can be sensitively detected by abnormal high intensity patterns.

In a time–frequency representation based on a windowed transform, such as the Gabor spectrogram, once the size of the window function is defined, the resolution will be fixed both in the time and frequency domains. This fixation may not be a disadvantage when all the features of interest have approximately the same time duration, or size, because a suitable window width can be chosen to match. However, a problem will occur if the features of a signal have differing sizes, because a single fixed resolution is incapable of satisfying the representation of different signal features. A recently developed wavelet

---

Received January 21, 1995; Accepted August 29, 1995.

Shock and Vibration, Vol. 3, No. 1, pp. 17–26 (1996)  
© 1996 John Wiley & Sons, Inc.

CCC 1070-9622/96/01017-10

transform uses a window function with a changing size so that not only one, but a series of resolutions can be applied to the windowed transform (Chui, 1992; Daubechies, 1992; Mallat, 1989). In the last 10 years, the applications of the wavelet transform have rapidly entered many areas of science and engineering. It has been demonstrated that if the wavelet transform is applied to the signals with local features, such as gear vibration signals from faulty gearboxes, it is capable of displaying different time sizes of features by a series of decomposed components or in a single distribution on a two-dimensional plane (Newland, 1993; Wang and McFadden 1993c, 1994). This provides a more powerful tool for describing all types of features of a mechanical signal.

Unlike the Fourier transform, in which only the trigonometric functions are the basis for decomposing a signal so that the result is unique, possible selections of wavelets for the decomposition basis are numerous. The criterion for choosing wavelets has brought about intensive discussions in the wavelet research community. It is believed that, in principle, the choice depends on the requirements of the particular applications. For example, for achieving maximum data compression and reconstruction, the orthogonal wavelet basis is used for image processing. But in detecting transients and displaying their intensity of energy in a time–frequency domain, the purpose of using wavelets is to compare the shape of the wavelet with transients of interest. In such a case, the main consideration is the level of similarity between the wavelet and the transients rather than any special relationships between each pair of wavelets, such as the orthogonality in the orthogonal wavelet basis.

In this article a unified description for the time–frequency and time–scale distributions will be given to show links among these transforms in different dimensional spaces. The wavelet family suggested by the author for detecting short-duration mechanical faults will also be presented with the results of using two distributions for gearbox fault diagnosis.

## A TIME–SCALE–FREQUENCY REPRESENTATION

Letting  $\tau$  be the time,  $f$  the frequency, and  $s$  the scale, signal  $x(\tau)$  is a time function and window  $w(\tau, f)$ , which in general is a complex function

and with a finite width of envelope, is assumed to be a function of time and frequency. The following equation defines a type of general form of the continuous wavelet transform (WT):

$$\text{WT}(t, f, s) = \int_{-\infty}^{\infty} x(\tau)c(s)w(s(\tau - t), f)d\tau \quad (1)$$

$$-\infty < t, f < \infty$$

where  $t$  is the analysis time indicating the central location of the window,  $f$  the frequency in the ordinary sense related to a sinusoidal oscillation inside the window envelope, and  $s$  the time–scale parameter ( $s \geq 0$ ) that magnifies and shrinks the window function along the time axis thus providing a changing width for the window.  $c(s)$  is a normalizing factor, a function of  $s$ .  $w(\tau, f)$  is then called a wavelet. Thus the transform  $\text{WT}(t, f, s)$  is a four-dimensional function or a distribution in the time–scale–frequency space. The corresponding wavelet family is generated by translation and dilation as

$$c(s)w(s(\tau - t), f). \quad (2)$$

Unlike an ordinary image in a two-dimensional plane, the distribution given by Eq. (1) generally does not give a clear visual effect because a four-dimensional pattern is not easily interpreted by human eyes. Several degenerated forms of Eq. (1) are used in practice.

## Grossmann and Morlet Wavelet Transform

In the general form described by Eq. (1), letting  $c(s) = \sqrt{s}$  and  $w(\tau, f) = w(\tau)$ , Grossmann and Morlet (1984) defined the wavelet transform as

$$\text{WT}(t, s) = \int_{-\infty}^{\infty} x(\tau) \sqrt{s} w(s(\tau - t))d\tau. \quad (3)$$

A signal  $x(\tau)$ , can be characterized by its decomposition onto the wavelet family, i.e., the transform decomposes the signal  $x(\tau)$  into a family of wavelets that are the translation and dilation of a unique-valued function  $w(\tau)$ . Because the integration acts as a filter and the wavelets with different scale  $s$  have different passbands in the frequency domain, a wavelet transform can also be interpreted as a decomposition of a signal into a set of frequency channels with different bandwidths. Figure 1 illustrates a process of dilation in a Gaussian enveloped oscillating wavelet fam-

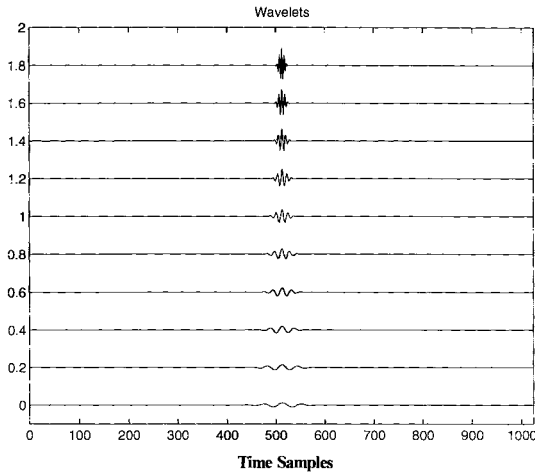


**FIGURE 1** Time width of wavelets narrows as scale increases.

ily. As the scale  $s$  increases, from the bottom to the top, the width of the wavelet becomes narrower. Figure 2 shows, from left to right, the corresponding Fourier spectra for the wavelets. As the scale  $s$  increases, the central frequency gets higher and the frequency band becomes wider. Choosing a series of scales, the decomposition will then be able to cover a full frequency range of interest.

An important particular case of the wavelet transform is that some wavelets  $w(\tau)$  exist such that the family is an orthogonal basis (Chui, 1992; Daubechies, 1992):  $\sqrt{2^j} w(2^j(\tau - 2^{-j}n))$  (where  $j, n$  are integers). Orthogonal wavelets, such as the well-known Daubechies wavelet series, offer fast

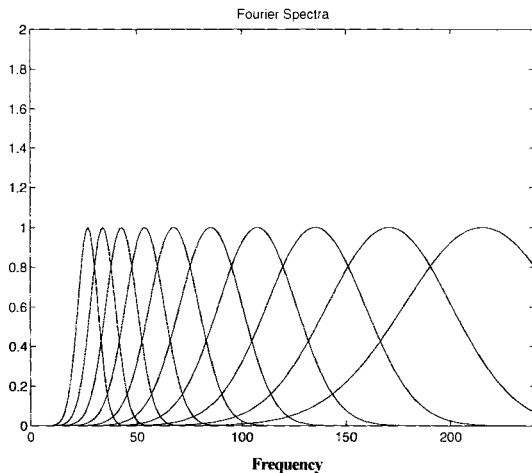


**FIGURE 2** Frequency width of wavelets expands with scale increases.

algorithms and no redundancy in the decomposition (Daubechies, 1992; Newland, 1993).

### Gaussian Enveloped Oscillating Wavelet Transform

A Gaussian shaped function is adopted as an envelope

$$h(\tau) = e^{-\sigma^2\tau^2} \quad (4)$$

where the constant  $\sigma \geq 0$ . The Gaussian enveloped oscillating (GEO) wavelet is defined as

$$w(\tau, f) = h(\tau)e^{-j2\pi f\tau} = e^{-\sigma^2\tau^2 - j2\pi f\tau}. \quad (5)$$

The wavelet family is now  $c(s)w(\tau, f) = c(s)e^{-\sigma^2s^2(\tau-t)^2 - j2\pi fs(\tau-t)}$ , and it consists of an envelope and an oscillation. The width of the envelope is adjusted by the scale parameter  $s$  and the basic frequency of oscillation is controlled by  $f$  in the complex function factor. This arrangement is rather simple, avoiding the difficult mixture of frequency and scale variables. In Eq. (1), letting  $c(s) = s$  and using the above wavelet, the wavelet transform is specified as

$$\text{WT}(t, f, s) = \int_{-\infty}^{\infty} x(\tau)se^{-\sigma^2s^2(\tau-t)^2 - j2\pi fs(\tau-t)}d\tau. \quad (6)$$

The normalizing factor  $s$  before the wavelet ensures an equal area is encircled, by the envelope and time axis, so that the intensity in both small and large sizes of the wavelet transform can be normalized. Unfortunately, this resulting four-dimensional function of the wavelet transform is hard to display and interpret in practical applications.

### Windowed Fourier Transform

If the scale is fixed to unity, i.e.,  $s = 1$ , implying that there is no dilation along the time axis and the window is fixed, Eq. (6) will be equivalent to a windowed Fourier transform:

$$\text{WT}(t, f) = e^{j2\pi ft} \int_{-\infty}^{\infty} x(\tau)e^{-\sigma^2(\tau-t)^2} e^{-j2\pi t\tau}d\tau \quad (7)$$

where the window is  $e^{-\sigma^2(\tau-t)^2}$  located at analysis time  $t$ . The extra factor  $e^{j2\pi ft}$  causes no change in the modules of  $\text{WT}(t, f)$ , but only in the phase.

By adjusting  $\sigma$ , the window width can be chosen to match the relatively short size of features in the analysed signal and to meet a compromised resolution in the time and frequency domain. The major advantage of using the windowed Fourier transform is that it gives a local enhancement for the signal section within the window. If by letting  $\sigma = 0$  and  $t = 0$ , corresponding to the case where the width of the Gaussian window is infinitely wide, the windowed Fourier transform degenerates to the ordinary Fourier transform:

$$\text{WT}(f) = \int_{-\infty}^{\infty} x(\tau)e^{-j2\pi f\tau}d\tau \quad (8)$$

where all sections of the signal are possible contributors for each spectral component and there is no indication when a specific spectral component takes place.

### Gabor Spectrogram

The windowed Fourier transform described in Eq. (7) is also called the Gabor transform, in which a signal in the time domain has been transformed into an *analysis time–frequency* domain. The analysis time  $t$  indicates the time position of the window. The result of the transform becomes a distribution on a time–frequency plane. From Eq. (7), the Gabor spectrogram (GS) is defined as

$$\begin{aligned} \text{GS}(t, f) &= |\text{WT}(t, f)|^2 \\ &= \left| \int_{-\infty}^{\infty} x(\tau)e^{-\sigma^2(\tau-t)^2-j2\pi f\tau}d\tau \right|^2. \end{aligned} \quad (9)$$

The Gabor spectrogram gives a simultaneous representation of signal components at all frequencies of interest and the sequence of their occurrence. Because the Gabor spectrogram emphasizes locally appearing components due to windowing, it is sensitive to local small changes, and thus is suitable for detecting those transients associated with early damage.

### Time-Scale Distribution

In the general form of the GEO wavelet in Eq. (5), if the frequency is fixed, i.e.,  $f = f_0 = \text{constant}$ , the wavelet transform becomes a three-dimensional function or a distribution on the time–scale plane:

$$\text{WT}(t, s) = \int_{-\infty}^{\infty} x(\tau)se^{-\sigma^2s^2(\tau-t)^2-j2\pi f_0s(\tau-t)}d\tau. \quad (10)$$

This time–frequency distribution is generally complex, but the module or the square of the module is usually taken for ease of display. This distribution reflects the level of similarities between the wavelet and signal resulting from the comparison over all time instants and scales, given by

$$\begin{aligned} \text{WS}(t, s) &= |\text{WT}(t, s)|^2 \\ &= \left| \int_{-\infty}^{\infty} x(\tau)se^{-\sigma^2s^2(\tau-t)^2-j2\pi f_0s(\tau-t)}d\tau \right|^2. \end{aligned} \quad (11)$$

The time–frequency distribution (9) and time–scale distribution (11) are two fundamental representations used for illustrating local features in mechanical signals. For obtaining higher resolutions, in the case of having different sizes of faults, the time–scale distribution is preferable because it possesses multiple resolutions. As the scale  $s$  takes different values, the wavelet changes, in both its width and oscillating frequency inside the envelope, to match all possible sizes of components in the signal. However, in the case where the local components to be detected have approximately the same size with a fixed window width, the time–frequency distribution can be applied with the advantage of an easy understanding of the frequency spectra.

Both the time–frequency (9) and time–scale distribution (11) provide an intensity distribution of the similarity over a two-dimensional plane. The magnitude of the intensity quantifies the similarity between the wavelet function  $e^{-\sigma^2\tau^2}e^{-j2\pi f\tau}$  and each part of the signal via the comparison with a single scale, and between the wavelet function  $e^{-\sigma^2(s\tau)^2}e^{-j2\pi f_0s\tau}$  and each part of the signal via the comparison with multiple scales, respectively.

## IMPLEMENTATION OF TRANSFORMS

### Time-Frequency Distribution

Using the Gabor transform, a signal in the time domain is transformed into the time–frequency domain. The whole distribution of the Gabor spectrogram represents components at all frequencies of interest and the sequence of their occurrence. Because the windowing has emphasized the local components, the closer the size of the window to the transient, the higher the sensitivity. In early gear damage detection, it is sug-

gested that the width of the window be equal to the time length covering one tooth pitch. In practical implementation of Eq. (9), the distribution takes a discrete form. The frequency  $f$  takes a finite number of values, i.e.,

$$\text{GS}(t, f_k) = \left| \int_{-\infty}^{\infty} x(\tau) e^{-\sigma^2(\tau-t)^2} e^{-j2\pi f_k \tau} d\tau \right|^2 \quad (12)$$

$$f_k = k f_b \quad (k = 0, 1, 2, \dots, M-1)$$

where  $f_k$  is the discrete frequency,  $f_b$  the half-power frequency bandwidth of the window, and  $M$  an integer. The interval  $f_b$  is determined by  $\sigma$ . Obviously,  $f_b$  and  $M$  must be suitably selected to cover a complete frequency range of interest with a cutoff frequency  $f_c = (M - \frac{1}{2})f_b$  without excessive overlap redundancy. Considering Eq. (12)

$$\int_{-\infty}^{\infty} x(\tau) e^{-\sigma^2(\tau-t)^2} e^{-j2\pi f_k \tau} d\tau$$

$$= \int_{-\infty}^{\infty} (x(\tau) e^{-j2\pi f_k \tau}) e^{-\sigma^2(\tau-t)^2} d\tau,$$

the convolution theorem, and the property of the symmetry  $e^{-\sigma^2(\tau-t)^2} = e^{-\sigma^2(t-\tau)^2}$ , the Gabor spectrogram becomes

$$\text{GS}(t, f_k) = |\mathcal{F}^{-1}[X(f + f_k)H(f)]|^2 \quad (13)$$

where  $\mathcal{F}$  represents the Fourier transform and  $\mathcal{F}^{-1}$  the inverse Fourier transform.  $H(f)$  is the Fourier transform of the envelope, given by

$$H(f) = \mathcal{F}[h(\tau)] = \frac{\sqrt{\pi}}{\sigma} e^{-(\pi/\sigma)^2 f^2}. \quad (14)$$

In the time domain, the half-power width of the above window is  $t_b = 1.18/\sigma$ , and in the frequency domain the half-power width is  $f_b = 0.375\sigma$ . Therefore, to cover the full frequency band of interest, the discrete frequency points are  $f_k = k f_b (k = 0, 1, 2, \dots, M-1)$ . The corresponding discrete form of Eq. (13) is

$$\widehat{\text{GS}}(n, f_k) = \left| \sum_{r=0}^{N-1} X(r + f_k) H(r) e^{j(2\pi r n / N)} \right|^2 \quad (15)$$

$$n = 0, 1, \dots, N-1$$

where  $N$  normally adopts a power of 2 for the convenience of carrying out the Fast Fourier Transform (FFT) calculations and  $M$  takes an integer of  $(fc/fb + 1/2)$ .

### Time-Scale Distribution

The GEO wavelet in Eq. (5) has a concentrated band in the frequency domain. This gives a continuous and simple pattern in the time-scale domain. It can be seen that the oscillating frequency  $f_0$  appears at the center of the frequency band of the wavelet. From Eq. (10), the time-scale distribution at a series of scale values is given by

$$W(t, s_k) = \left| \int_{-\infty}^{\infty} x(\tau) s_k e^{-\sigma^2 s_k^2 (\tau-t)^2 - j2\pi f_0 s_k (\tau-t)} d\tau \right|^2 \quad (16)$$

where  $s_k$  is the discrete scale value. Suitable selection of  $s_k$  and  $f_0$  can allow the wavelet series to cover all frequencies of interest. It is easy to know that the half-power wavelet width is  $t_b^{(k)} = 1.18/(s_k \sigma)$ , and in the frequency domain,  $f_b^{(k)} = 0.375 s_k \sigma (k = 1, 2, \dots, M; M$  may be chosen to satisfy  $2^M = N)$ . It is suggested that  $s_k$  and  $f_0$  are chosen to let the central frequencies of the wavelets have octave band intervals (for example,  $\lambda = 1/3$ ). Let the scale  $s_1 = 2^\lambda - 1$ , then  $s_k = 2^{(k-1)\lambda} (2^\lambda - 1) (k = 1, 2, \dots, M)$ . The central frequency of wavelets is  $f_0^{(k)} = s_k f_0$ . If  $f_c$  is the cutoff frequency, using the condition of half-power point overlap  $f_0^{(k)} + \frac{1}{2} f_b^{(k)} = f_0^{(k+1)} - \frac{1}{2} f_b^{(k+1)}$ , and the cutoff frequency  $f_c = f_0^{(M)} + \frac{1}{2} f_b^{(M)}$ , it can be found that the parameter  $\sigma = 2.667 \cdot 2^{-M\lambda} f_c$  and the base frequency  $f_0 = 0.1874\sigma \cdot (2^\lambda + 1)/(2^\lambda - 1)$ .

Because the GEO wavelet satisfies  $w(-\tau) = \bar{w}(\tau)$ , we have

$$\int_{-\infty}^{\infty} x(\tau) w(s_k(\tau - t)) d\tau$$

$$= \int_{-\infty}^{\infty} x(\tau) (e^{-\sigma^2 s_k^2 (t-\tau)^2 + j2\pi f_0 s_k (t-\tau)}) d\tau$$

$$= \int_{-\infty}^{\infty} x(\tau) \bar{w}(s_k(t - \tau)) d\tau.$$

Using the convolution theorem of the Fourier transform, Eq. (16) can be written as

$$W(t, s_k) = \left| s_k \mathcal{F}^{-1} \left( X(f) \bar{W} \left( \frac{f}{s_k} \right) \right) \right|^2. \quad (17)$$

Because  $\mathcal{F}(\overline{w}(\tau)) = \overline{W}(f) = (\sqrt{\pi}/\sigma)e^{-(\pi/\sigma)^2(f+f_0)^2}$ , the wavelet transform (17) can be written as

$$W(t, s_k) = \left| \frac{\sqrt{\pi}}{\sigma} \mathcal{F}^{-1}(X(f)e^{-(\pi/\sigma)^2(f/s_k+f_0)^2}) \right|^2 \quad (18)$$

This has brought about the important result that using the GEO wavelet, the calculation of the wavelet transform can also be implemented by a series of Fourier transforms, taking advantage again of the efficiency of the FFT algorithm. The corresponding discrete form of Eq. (17) is

$$\hat{W}(n, s_k) = \left| \sum_{r=0}^{N-1} X(r) \overline{W}\left(\frac{r}{s_k}\right) e^{j(2\pi rn/N)} \right|^2 \quad (19)$$

$$n = 0, 1, \dots, N-1.$$

The wavelet family  $se^{-\sigma^2 s^2(\tau-t)^2 - j2\pi f_0 s(\tau-t)}$  is illustrated in Fig. 1, which simulates the transients with all oscillating frequencies by changing the scale factor. Figure 2 shows that the Fourier spectra of all scales of wavelets sequentially cover all the frequencies of interest. When a signal is decomposed onto one of these wavelets, a large value will be obtained if there is a transient with a similar shape of the wavelet. Therefore, the wavelet family can be used to detect all sizes of transients in the signal, such as all types of faults on a whole gear profile.

## Computing

Computing the time–frequency or time–scale distribution only takes one FFT for the vibration signal with  $N$  samples and  $M$  inverse FFTs with a length of  $N$ . The wavelet transforms described in Eqs. (15) and (19) have been implemented by computer programs written in MATLAB and C language running on an IBM PC-AT compatible computer and a SUN SPARC station. The function  $\hat{G}\hat{S}(n, f_k)$  of Eq. (15) and  $\hat{W}(n, s_k)$  of Eq. (19) are calculated for typical  $M = 10$  discrete frequencies or scales, corresponding to  $N = 1024$  time samples. The resulting distributions may be displayed as contours on a two-dimensional chart with  $N \times M$  pixels. More details may be obtained from the distribution patterns if a smaller increment in the central frequency and a larger  $M$  are chosen to produce a transform at more frequencies or scales, but at a cost of more FFT calculation time.

## GEARBOX DIAGNOSIS

The information about the gear condition is expected to be carried by the time domain synchronous average (McFadden, 1986) of the casing vibration signal. However, clear symptoms may not be observed, particularly in the early stages, and little other further information about the nature of the fault can be seen directly from the average. Early damage to a gear tooth causes only a short-duration variation in the vibration signal, which lasts less than one tooth meshing period and normally takes the form of modulated or unmodulated oscillation. In later stages, with the duration of the abnormal variation becoming longer, two or more tooth meshing periods may be affected. Other distributed faults like eccentricity and wear normally cover a large part or even the whole revolution of the gear. Therefore, possible faults may appear in many different size components in the vibration signal.

Damage on a gear tooth normally starts with a small crack or spalling, which produces a short-duration disturbance in the time history of the associated vibration signal. In the time–frequency and time–scale distribution, an abnormal peak will appear in the distribution corresponding to the damage. The time signal, when displayed on a two-dimensional plane, will be able to give comprehensive information about the nature of the fault. A typical form of the pattern is a high peak or strip across a band of frequencies around the meshing frequency and its harmonics or across a range of scales. Sometimes several such peaks may be caused by the same fault, and this can be identified by its same time appearance. The features of the pattern in the distribution quantify the nature of the fault. Wang and McFadden (1993b) introduced image processing techniques to segment and identify the feature of these patterns from high-intensity zones.

Ideally, the general form of the wavelet transform (6) would give an intensity distribution of the similarity in the time–scale–frequency space, including all possible choices for the width of the window (adjusted by the scale parameter  $s$ ) and the oscillating frequencies ( $f$ ). But the difficulty lies in the display of such a four-dimensional function as mentioned before; a compromise in resolution must be made. The alternative is to use either the time–frequency distribution with a fixed window or the time–scale distribution with a fixed basic frequency that provides the intensity distribution on an easily displayed two-di-

dimensional plane. For diagnosing all possible different types of gear faults, the time-scale distribution should be adopted because it has a changing width window. On the other hand, if only one type of fault is of particular interest, such as small cracks, only one level of resolution is required and a fixed width window matching the size of the fault can be adopted, so that the time-frequency distribution can be applied, which keeps the ordinary frequency meanings easily interpreted.

## RESULTS OF DIAGNOSIS

There are four gears in the experimental gearbox. An accelerometer is mounted on the gearbox casing, and a synchronous impulse generator is used to record the position of the input shaft. After passing through an antialiasing filter, the acceleration and the synchronous signal are connected to a multiple channel analogue to digital converter inserted in an IBM 486DX compatible PC. Software is used for synchronous averaging and further analysis. The upper curve in Fig. 3 shows the average of the casing vibration synchronized to a gear of 20 teeth on the input shaft in normal condition; 1024 samples are obtained by interpolation to cover exactly one revolution of the gear.

By removing the fundamental and harmonics of the tooth meshing frequency (20 orders), the residual signal shown by the lower curve in Fig. 3 is obtained, representing the difference between the actual tooth shape and that of the average tooth shape. There is no obvious indication of

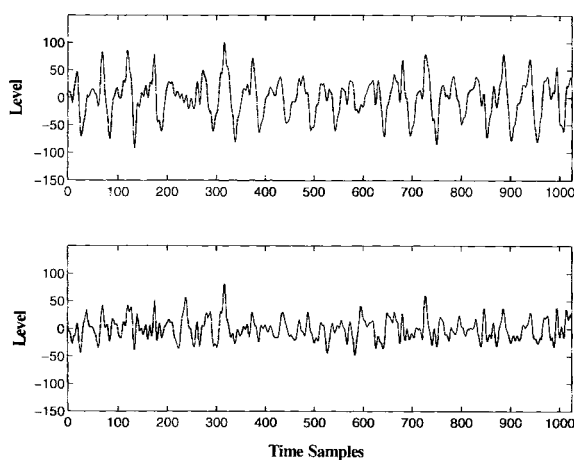


**FIGURE 3** Synchronous averaged vibration and its residual.

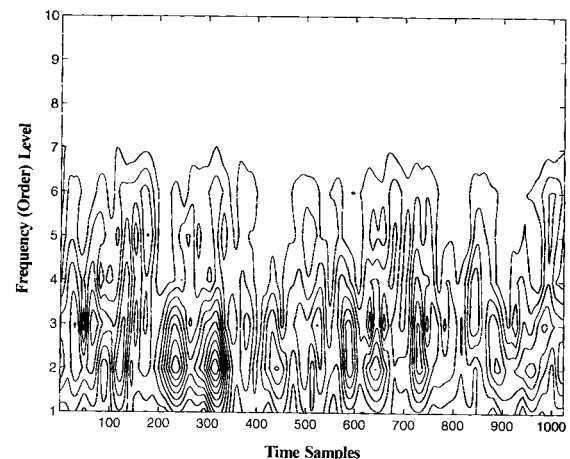


**FIGURE 4** Time-frequency distribution (normal condition).

any tooth damage at this stage. Figure 4 is the Gabor spectrogram for the residual signal. The 10 levels along the vertical axis linearly represents the central frequencies of the bands ranging from 0 to 240 orders. They are 0, 24, 48, 72, 96, 120, 144, 168, 192, and 216 orders, respectively. At the locations around time samples 230 and 310, there are two relatively strong peaks at low frequencies, indicating possible unsatisfactory manufacturing or assembly faults of the gear. Figure 5 is the time-scale distribution for the residual signal. These 10 scales give 10 central frequency locations of one-third octave bands. These central frequencies are 27, 34, 43, 54, 68, 85, 108, 136, 171, and 215 orders, respectively. Each pair of adjacent bands are overlapped at their com-

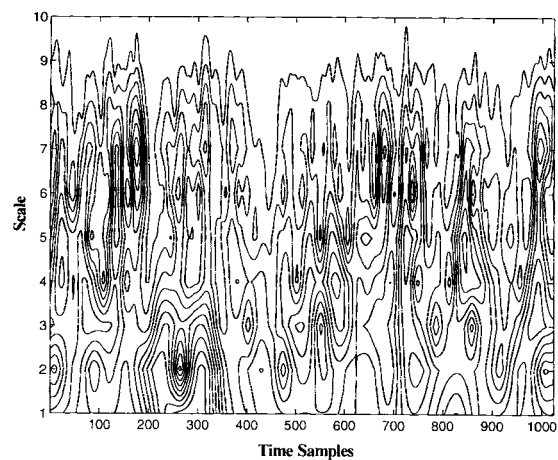


**FIGURE 5** Time-scale distribution (normal condition).

mon half-power points, and these 10 bands have fully covered the frequencies ranging from 22 to 240 orders. Due to the variations among the teeth caused by normal manufacturing errors and other synchronous noise resources (such as noise from the belt drive wheel on the input shaft), vast patterns appear at all scales; but there is no dominant peak in the whole distribution, showing that no damage has occurred. The patterns appearing at higher levels present a lot of fine details. Comparing with the Gabor spectrogram where only one resolution is used for describing the small and large size of the features, the time-scale distribution gives multiple resolutions so that different sizes of details in the analysed signal have been described effectively from low to high scales. Small variations can be found in the higher scale area. Nevertheless the distribution is rather uniform and flat, confirming that the gear is in normal condition. At low values of  $s$ , where large sizes of variations in the signal should be apparent, the distribution is also relatively uniform during the whole revolution.

A cut 2.5 mm long and 0.2 mm depth and width on one side of a tooth surface is made on a spare identical gear to simulate damage. The upper curve in Fig. 6 shows the time domain average for the vibration. A burst can be easily seen around the time sample 930. After removal of the fundamental and harmonics, the residual signal is shown by the lower curve of Fig. 6. Because the fundamental and harmonics are relatively low and the background noise is relatively high, the two curves are not very different in appearance. Figure 7 is the Gabor spectrogram for the resid-

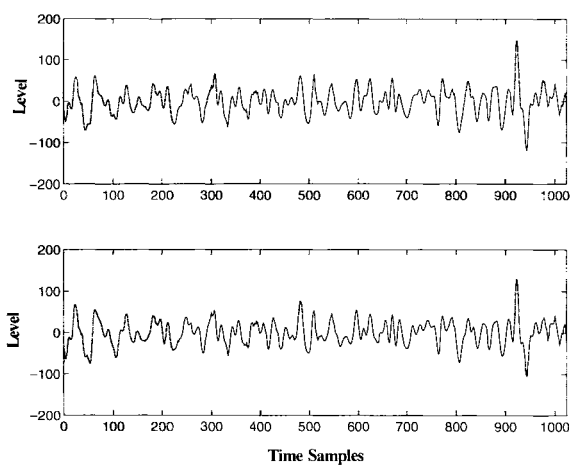


**FIGURE 6** Synchronous averaged vibration and its residual.

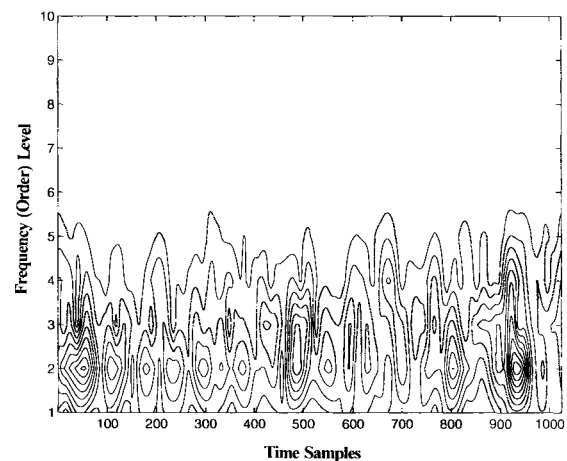


**FIGURE 7** Time-frequency distribution (faulty condition).

ual signal. A strong peak appears at the sample 930, covering frequency levels 1–5, indicating the existence of a sharp impulse. Figure 8 represents the square of the absolute values, providing a higher contrast for showing the damage at the same location. Figure 9 is the time-scale distribution for the corresponding signal. Using absolute values, clear peaks near the sample 930 show the details of the damage. At large values of the scale (6–10), some short-duration variations appeared that describe the tiny size defects on the tooth meshing faces. In particular, at samples 850 and 980, two narrow high-frequency patterns appear, indicating there are two significant small defects. Figure 10 represents the square of the absolute values, providing again a higher con-

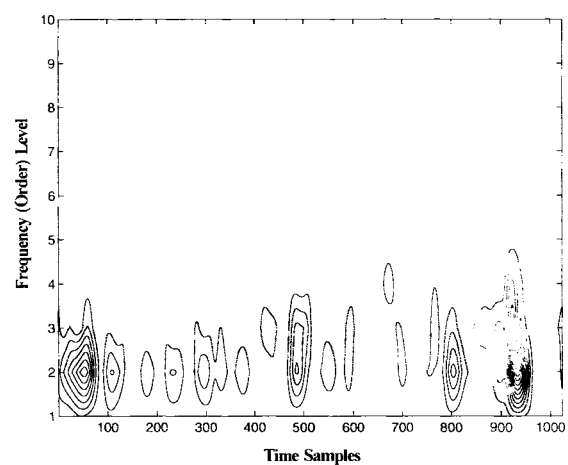


**FIGURE 8** Square of time-frequency distribution (faulty condition).



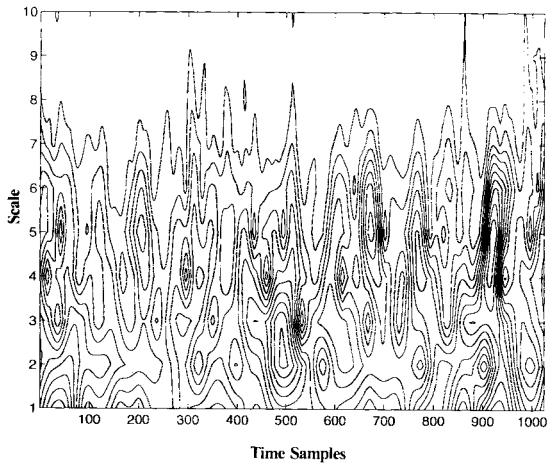


**FIGURE 9** Time-scale distribution (faulty condition).

trast for showing the damage at the same location.

## DISCUSSION

The style in which the scale is changed can be linear or nonlinear in the time-scale representation to cover the desired frequency range. Octave bands cover wider frequency and possess reasonable frequency increments. However, this may not be as straightforward as in the time-frequency distribution of the Gabor spectrogram, where image processing techniques can be easily applied for pattern interpretation (Wang and McFadden, 1993a,b).

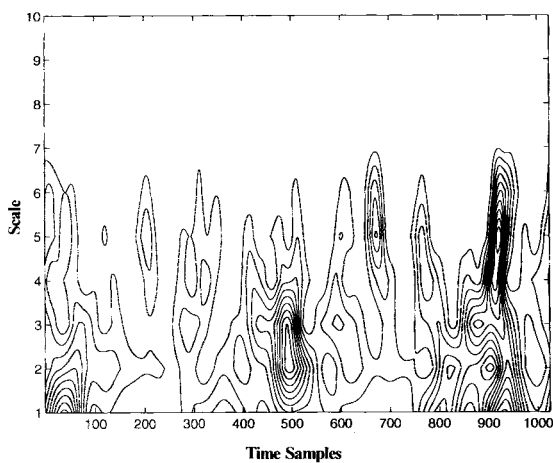


**FIGURE 10** Square of time-scale distribution (faulty condition).

For detecting the transients, if orthogonal wavelets are applied, due to their restricted and special shapes and limited number of scales, it may be hard to find any significant similarities between the wavelet and the transients. In addition, the frequency contents of the orthogonal wavelet are separately distributed over the frequency axis. The intensity distribution of the transform does not have enough suitable scales for matching and describing the details about the transient nature, either large or small size. The jump of orthogonal wavelet locations makes the transform pattern time variant, i.e., the same transient at different locations on the time axis could have different patterns in the transform distribution. In local feature detection, a small change in the vibration signal may remove the chance of matching the wavelet of the same size at the closet time during the transform and so be weak or unable to be seen in the time-scale distribution chart. However, orthogonal wavelets give a smart inverse transform to reconstruct the original time signal without redundancy. The nonorthogonal wavelets suggested in this article look efficient in decomposition rather than reconstruction.

Because the selection of wavelet type depends on the task of signal analysis, if more types of wavelets are required for disclosing different shapes of local features, in implementing automated diagnosis the time-scale distribution generated from the wavelet transform may need to be inspected and interpreted by a sophisticated system because a different wavelet family may give a completely different distribution in the time-scale domain.

In implementing the wavelet transform, the FFT is used as a short cut for the algorithm. In more general cases, such an advantage will not be naturally provided.

## CONCLUSION

A general form of time-frequency-scale distribution of the wavelet transform and the relationship with other distributions were discussed. The Gaussian enveloped oscillating wavelet is suggested to analyze local features in the vibration signals produced by faults. It was shown by examples that the time-frequency and time-scale distributions generated by the wavelet transform are effective in presenting and analyzing the local

features of vibration signals so that the mechanical systems can be diagnosed.

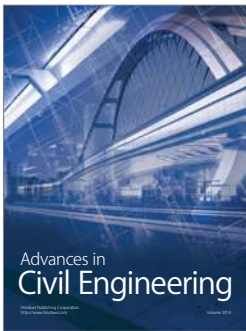
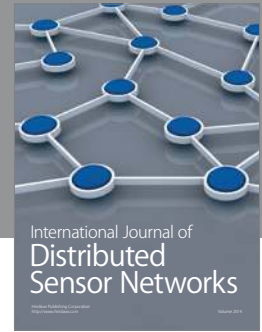
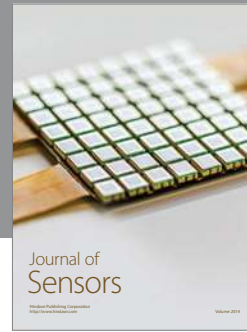
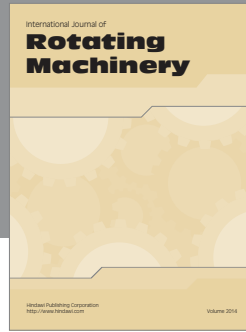
The essence of selecting the wavelet family to calculate the time–scale distribution is to find a suitable function to simulate the short-duration components of interest. Therefore, the transform gives a high absolute value, if at a certain scale and time there is a similarity between the wavelet and the analysed signal; otherwise it gives a low absolute value.

The time–frequency distribution is easily interpreted and is suitable for detecting single size faults. The time–scale distribution is preferable when detecting different sizes of faults because it has multiple resolutions and simultaneously displays the large and small size features of a signal, enabling a simultaneous detection of both large and small size faults, or distributed and localized faults. In the implementation of the time–scale distribution, one-third octave bandwidths of the wavelets and the half-power points of overlapping are adopted to ensure that the frequencies in the band of interest are not missed by a limited number of scales; and meanwhile excessive redundancy of computation for the transforms is avoided.

The author wishes to thank Mr. Christof Spies for his work in the experiment.

## REFERENCES

- Chui, C. K., 1992, *An Introduction to Wavelets*, Academic Press, Boston.
- Classen, T. A. C. M., and Mecklenbräuker, W. F. G., 1980, "The Wigner Distribution—A Tool for Time–Frequency Signal Analysis, Part 3: Relations with Other Time–Frequency Signal Transformations," *Philips Research Journal*, Vol. 35, pp. 372–389.
- Daubechies, I., 1992, *Ten Lectures on Wavelets*, Society for Industrial and Applied Mathematics, Philadelphia.
- Grossmann, G., and Morlet, G., 1984, "Decomposition of Hardy Functions into Square Integrable Wavelets of Constant Shape," *SIAM Journal of Mathematics*, Vol. 15, pp. 723–736.
- Mallat, S. G., 1989, "Multifrequency Channel Decompositions of Images and Wavelet Models," *IEEE Transactions on Acoustics, Speech and Signal Processing*, Vol. 37, pp. 2091–2110.
- McFadden, P. D., 1986, "Detecting Fatigue Cracks in Gears by Amplitude and Phase Demodulation of the Meshing Vibration," *American Society of Mechanical Engineers Transactions, Journal of Vibration Acoustics Stress and Reliability in Design*, Vol. 108, pp. 165–170.
- Newland, D., "Discrete Wavelet Analysis," in *An Introduction to Random Vibration, Spectral and Wavelet Analysis*, 1993, Wiley, New York, pp. 295–370.
- Wang, W. J., and McFadden, P. D., 1993a, "Early Detection of Gear Failure by Vibration Analysis—I. Calculation of the Time–Frequency Distribution," *Mechanical Systems and Signal Processing*, Vol. 7, pp. 193–203.
- Wang, W. J., and McFadden, P. D., 1993b, "Early Detection of Gear Failure by Vibration Analysis—II. Interpretation of the Time–Frequency Distribution Using Image Processing Techniques," *Mechanical Systems and Signal Processing*, Vol. 7, pp. 205–215.
- Wang, W. J., and McFadden, P. D., 1993c, "Application of the Wavelet Transform to Gearbox Vibration Analysis," *The ASME Structural Dynamics and Vibration, The 16th Annual Energy—Sources Technology Conference and Exhibition*, January 31–February 3, ASME, Houston, TX, Vol. 52, pp. 15–20.
- Wang, W. J., and McFadden, P. D., 1994, "Application of Wavelets in Non-stationary Vibration Signal Analysis for Early Gear Damage Diagnosis," *Proceedings of the International Conference on Vibration Engineering (ICVE '94)*, 1994, Beijing: International Academic Publishers, pp. 615–620.



**Hindawi**

Submit your manuscripts at  
<http://www.hindawi.com>

